A comparison of hydrographically and optically derived mixed layer depths

David G. Zawada[1] and J. Ronald V. Zaneveld

WET Labs, Inc., Philomath, Oregon, USA

Emmanuel Boss

School of Marine Sciences, University of Maine, Orono, Maine, USA

Wilford D. Gardner, Mary Jo Richardson, and Alexey V. Mishonov

Department of Oceanography, Texas A&M University, College Station, Texas, USA

[1] Efforts to understand and model the dynamics of the upper ocean would be significantly advanced given the ability to rapidly determine mixed layer depths (MLDs) over large regions. Remote sensing technologies are an ideal choice for achieving this goal. This study addresses the feasibility of estimating MLDs from optical properties. These properties are strongly influenced by suspended particle concentrations, which generally reach a maximum at pycnoclines. The premise therefore is to use a gradient in beam attenuation at 660 nm (c660) as a proxy for the depth of a particle-scattering layer. Using a global data set collected during World Ocean Circulation Experiment cruises from 1988–1997, six algorithms were employed to compute MLDs from either density or temperature profiles. Given the absence of published optically based MLD algorithms, two new methods were developed that use c660 profiles to estimate the MLD. Intercomparison of the six hydrographically based algorithms revealed some significant disparities among the resulting MLD values. Comparisons between the hydrographical and optical approaches indicated a first-order agreement between the MLDs based on the depths of gradient maxima for density and c660. When comparing various hydrographically based algorithms, other investigators reported that inherent fluctuations of the mixed layer depth limit the accuracy of its determination to 20 m. Using this benchmark, we found a ~70% agreement between the best hydrographical-optical algorithm pairings.

Citation: Zawada, D. G., J. R. V. Zaneveld, E. Boss, W. D. Gardner, M. J. Richardson, and A. V. Mishonov (2005), A comparison of hydrographically and optically derived mixed layer depths, *J. Geophys. Res.*, *110*, C11001, doi:10.1029/2004JC002417.

1. Introduction

[2] Created by the confluence of atmospheric and radiational forces, the oceanic upper mixed layer is of importance to many oceanographic disciplines. Defined as being quasi-homogeneous in salinity and temperature [*Kara et al.*, 2000; *Price et al.*, 1986], this layer plays an integral part in air-sea interactions through the storage and exchange of heat, gases, momentum, and freshwater [*Ali and Sharma*, 1994; *Kraus and Businger*, 1994]. Oscillations in the depth of this layer, that is, the mixed layer depth (MLD), influence the vertical distribution of biological, chemical, and particulate components in surface waters [*Gardner et al.*, 1995]. In

addition, biological productivity is proportional to the MLD [*Behrenfeld and Falkowski*, 1997].

[3] Given its importance, measuring the MLD on basin-wide scales would be of great value to oceanographic and atmospheric scientists. Configuring an airborne or space-borne remote sensing platform is a natural choice. A few studies have addressed the potential of this approach. They include the use of airborne light detection and ranging (lidar) systems [*Hoge et al.*, 1988; *Lee et al.*, 2002], the Advanced Very High Resolution Radiometer (AVHRR) satellite [*Yan et al.*, 1990], the GEOSAT satellite altimeter [*Ali and Sharma*, 1994], and an assimilative technique combining sea surface height, salinity, and temperature [*Durand et al.*, 2003]. Implicit in each of these techniques is the derivation of mixed layer depths from a remotely detectable parameter, such as the depth of subsurface particle-scattering layers (lidar), sea surface temperature (AVHRR), or changes in sea level (GEO-SAT). Because these techniques are based on different parameters, the identification and quantification of the

---

[1]Now at Center for Coastal and Watershed Studies, U.S. Geological Survey, St. Petersburg, Florida, USA.
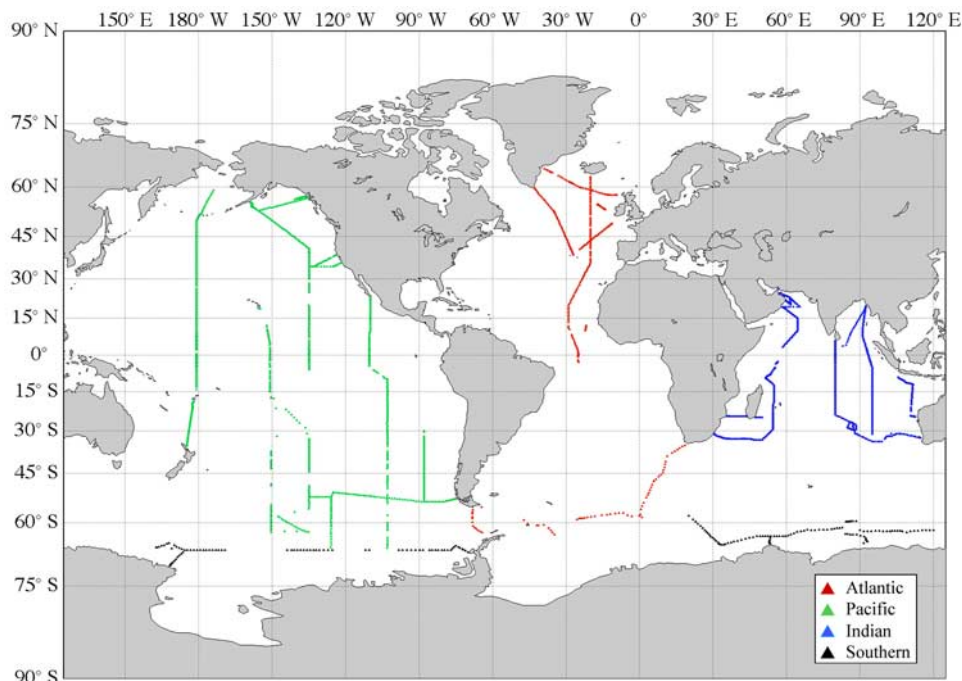
Figure 1. WOCE sampling sites. Collection sites for the data used in this study are marked.

MLD are highly method dependent. Additional uncertainty arises from the absence of a standardized, precise definition of the MLD.

[4] One faces the same challenges even when using in situ data. Numerous algorithms exist for determining the MLD from hydrographical measurements. The most commonly used algorithms require vertical profiles of either temperature or density. Several authors provide discussions and examples of the various MLD definitions [*Brainerd and Gregg*, 1995; *Kara et al.*, 2000; *Lukas and Lindstrom*, 1991]. As this study demonstrates, predicted MLD values can differ by an order of magnitude.

[5] Our objective is to investigate the feasibility of using an optical technique for estimating the mixed layer depth. The reason why we expect optical properties to be correlated with the mixed layer depth pertains to the particle distribution in the upper ocean. The vertical structure of particulates is the result of many processes. Some of these are purely physical, such as advection and mixing, while others are biological, such as phytoplankton-related processes (e.g., growth, swimming, and sinking). Processes indirectly affecting particle distributions include the advection and mixing of nutrients and the vertical structure of irradiance, which depends on the nature and the distribution of the particulates and dissolved materials, which in turn depend on the processes mentioned above. The activity of predators is difficult to estimate a priori. The timescales for the biological and physical processes are different as well. In general, the biogeochemical and physical forcing functions in the mixed layer are different from those deeper in the ocean. We therefore anticipate a difference in biogeochemical parameters above and below the pycnocline. Since these differences manifest themselves as differences in optical parameters, we expect to see differences in optical properties above and below the pycnocline.

[6] To achieve global coverage, we used hydrographic and optical property profiles that were collected as part of the World Ocean Circulation Experiment (WOCE, see http://whpo.ucsd.edu/) from 1988–1997. MLDs were computed from either temperature or density profiles by six algorithms and compared to MLDs derived only from optical data. Since there are no published algorithms for calculating mixed layer depths from inherent optical properties of seawater, two of the hydrographic methods were adapted for this purpose. Comparisons were made to determine the highest correlation between a hydrographically based and optically based algorithm. We note that while an extensive data set was used, it is limited in both geographical and seasonal coverage.

2. Methods

[7] All of the algorithms discussed below were implemented in MATLAB™ version 5.2.1 on an Apple Macintosh with a 450 MHz PowerPC G3 CPU.

2.1. WOCE Data Set

[8] Data sets from 1988–1997 are available that contain both CTD and beam transmissometer measurements (CTD data are available on the Web at http://whpo.ucsd.edu/; transmissometer data are available at http://oceanography.tamu.edu/%7Epdgroup/DataDir/SMP-data.html). Data from 2,085 sampling stations spanning the world ocean (Figure 1) were analyzed in this study. Each record includes vertical profiles of temperature, salinity, and beam transmission measured at 2 m intervals. Sampling was performed evenly in terms of time of day. On a seasonal basis, however, data collection primarily took place between the months of February and August (Figure 2). Most of the samples were collected between 1992–1995.
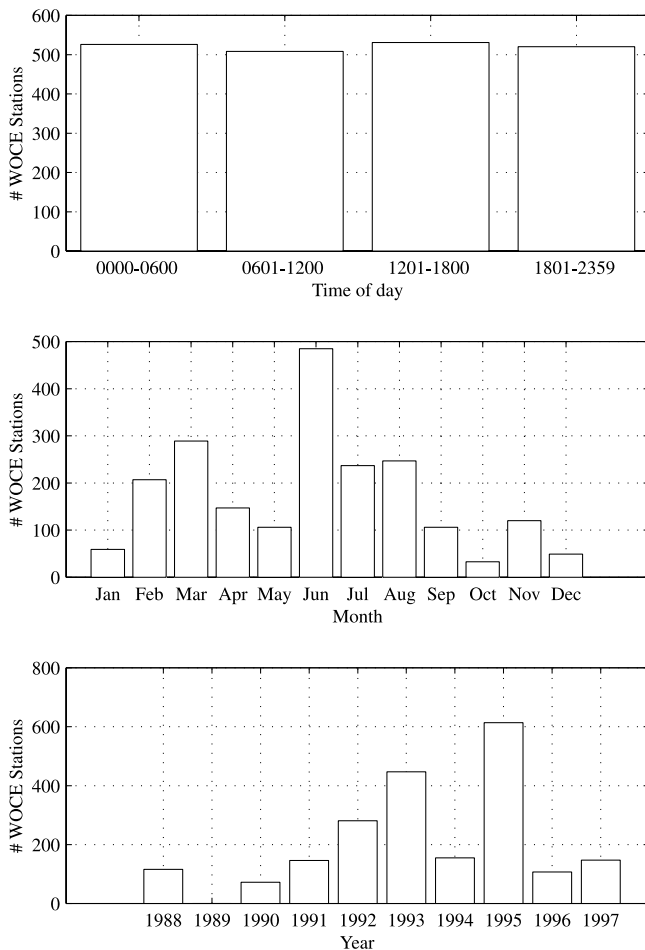
Figure 2. Distributions of sample collection times. The three plots show the distributions of collection times for the 2085 records analyzed in this study. Histograms are presented for time of day, month of the year, and year.

[9] The beam transmission values were measured at 660 nm and converted to the total beam attenuation coefficient (c) according to the expression

$$c = -\frac{\ln(T/100)}{z},$$ (1)

where c is the total beam attenuation coefficient (m^{-1}), T is the transmission (%), and z is the beam path length (m). We used total beam attenuation coefficient at 660 nm ($c660$) instead of beam transmission because $c660$ is more relevant to the issue of remotely measuring mixed layer depths. Ideally, one would use the backscattering coefficient (b_b). However, the WOCE data set only provides profiles of c. Fortunately, the total beam attenuation coefficient at 660 nm is an excellent proxy for particle concentration [*Pak et al.*, 1988]. The total beam attenuation coefficient represents the summation of the beam attenuation coefficients for seawater (c_w), dissolved organic matter or "yellow matter" (c_y), and particles (c_p). Mathematically, this is expressed as

$$c = c_w + c_y + c_p.$$ (2)

Since c_w may be regarded as a constant and $c_y(660)$ is negligible, except in turbid waters, changes in c are largely attributable to changes in particle concentration. Particulate beam attenuation is dominated by scattering, but absorption also plays a role. In mathematical terms,

$$c_p = a_p + b_p, \quad b_p = b_{p_f} + b_{p_b},$$ (3)

where a_p denotes absorption by particles and b_p corresponds total scattering, which has both forward (b_{p_f}) and backward (b_{p_b}) components. For determining mixed layer depths by optical means, particulate backscattering (b_{p_b}) is the component of interest. Although absorption by phytoplankton will affect c_p, at 660 nm scattering dominates absorption, often by a factor of $2-3$. To a first order, variability in $c660$ is a measure of variability in particulate scattering. Hence we expect a gradient in $c660$ to manifest itself as a gradient in $b_{p_b}(660)$ as well.

2.2. Algorithms for Computing MLD on the Basis of Hydrographic Data

[10] Numerous algorithms exist for computing mixed layer depths from temperature or density profiles. Most of these methods use criteria based on either a fixed difference from the surface value or a gradient in excess of a specific value to determine the MLD [*Lukas and Lindstrom*, 1991; *Brainerd and Gregg*, 1995; *Kara et al.*, 2000]. Temperature-based techniques have been used most frequently, owing to the ease of reliably measuring temperature. For regions with weak haloclines, both the temperature- and density-based techniques produce nearly equivalent results [*Brainerd and Gregg*, 1995]. However, density-based methods are more reliable for regions subject to intense freshwater input or where salinity is important for stabilizing the upper water column, such as in the sub-Arctic [*Brainerd and Gregg*, 1995; *Levitus*, 1982; *Lukas and Lindstrom*, 1991] or where evaporation can destabilize the mixed layer [*Lee et al.*, 2000; *Gardner et al.*, 1999]. *Kara et al.* [2000] found their density-based technique consistently better at predicting MLD than their temperature-based analog. In this study, MLDs were computed using one temperature-based and five density-based algorithms. An overview of each method is presented below. Details may be found in the cited references. To avoid any possible bias due to short-term surface effects, such as diurnal heating, profile data above a 10 m depth were omitted from analysis.

2.2.1. Method 1: Kara Isothermal Layer Depth (ILD)

[11] This method belongs to the temperature difference category. Unlike similar approaches, *Kara et al.* [2000] provide quantitative analysis justifying the selection of an optimal ΔT criterion of 0.8 °C. Starting with the reference temperature at 10 m, T$_{ref}$, adjacent temperatures in the profile are compared until a difference >0.1ΔT is found. T$_{ref}$ is then set to the temperature at the shallower of the two depths. The ILD is determined to be the depth at which the temperature has changed by an absolute value of ΔT from the updated T$_{ref}$. If no depth range is found within which the temperature change is >0.1ΔT, the profile is searched again, looking for a temperature change of ΔT relative to the temperature at 10 m. If found, the ILD is set to this depth, otherwise, it is set to the depth at the bottom of the profile.
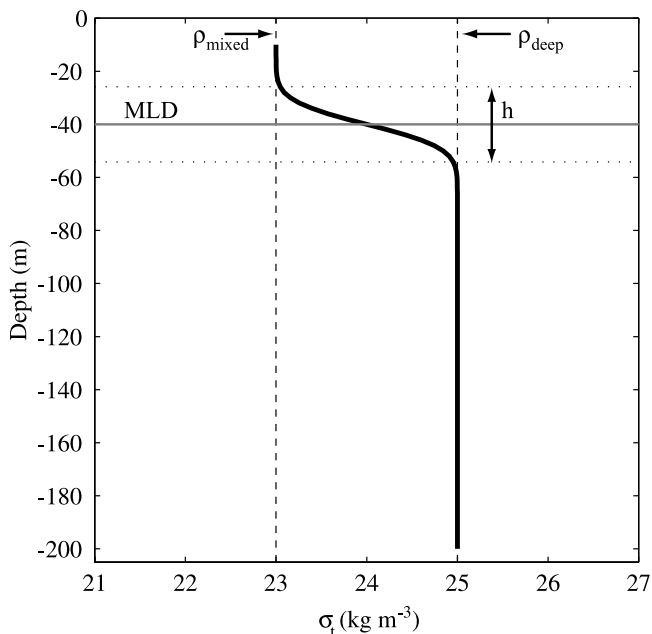
Figure 3. Idealized density profile. The Steyn method for determining the MLD fits an idealized profile to an observed one. The densities ρ_{mixed} and ρ_{deep} correspond to the mixed layer and deep water portions of the profile, respectively. The thickness of the transition zone (h) is the distance between the mixed layer and deep water.

2.2.2. Method 2: Kara Density Difference (Kara)

[12] This method follows an analogous procedure to that of method 1. A density profile is generated from the WOCE temperature and salinity data, using the equation of state for seawater developed by *Millero and Poisson* [1981]. The density variation, $\Delta\sigma_t$, is determined from the temperature change, ΔT, in the equation of state

$$\Delta\sigma_t = \sigma_t(T + \Delta T, S, P) - \sigma_t(T, S, P), \qquad (4)$$

where S is salinity and P is the pressure, which is set to zero. For convenience, density (ρ) is expressed as $\sigma_t = \rho - 1000$ (kg m^{-3}). As with the ILD, ΔT was set to 0.8 °C.

2.2.3. Method 3: Lukas-Lindstrom Fixed Density Gradient (fxGrad)

[13] *Lukas and Lindstrom* [1991] use a density gradient criterion of 0.01 kg m^{-4} to define the MLD. Starting with "surface" (i.e., 10 m) values, the density profiles computed as part of method 2 were searched until the gradient criterion was exceeded between adjacent 2-m data points. The MLD was taken to be the shallower of the two depths in the interval.

2.2.4. Method 4: Levitus Density Difference (Lev)

[14] *Levitus* [1982] defines the MLD to be the depth at which $\Delta\sigma_t = 0.125$ kg m^{-3}, relative to the surface density, that is, the density at 10 m.

2.2.5. Method 5: Maximum Density Gradient (Grad)

[15] The WOCE temperature and salinity data were used to generate a corresponding density profile, according to the equation of state for seawater [*Millero and Poisson*, 1981]. This profile was smoothed with a five-point moving average and used to compute the density gradient. The depth of the maximum absolute gradient magnitude, max $|\Delta\sigma_t/\Delta z|$, was considered to be the MLD. While this is not a standard hydrographic definition, oceanic particle distribution is often closely related to the density structure. Therefore this definition was added to the suite of MLD algorithms.

2.2.6. Method 6: Steyn Ideal Fit (Steyn)

[16] This algorithm was developed to detect atmospheric mixed layer structures from lidar backscattering profiles [*Steyn et al.*, 1999]. In lieu of backscattering data, this technique has been adapted to utilize density profiles and $c660$ profiles. The strategy is to fit an idealized profile, $\rho(z)$, to an observed profile, $\rho_{obs}(z)$, by minimizing an error condition or cost function. One might argue that such a procedure presupposes the existence of an idealized profile. However, Steyn et al. state that the method will only detect mixed layers in profiles resembling the chosen ideal. As will be shown with examples, the formulation of the idealized profile is sufficiently robust to cope with extreme profile shapes.

[17] The equation for the idealized profile used in this study is

$$\rho(z) = \frac{\rho_{mixed} + \rho_{deep}}{2} - \frac{\rho_{mixed} - \rho_{deep}}{2} \, erf\left(\frac{z - MLD}{h}\right), \qquad (5)$$

where ρ_{mixed} and ρ_{deep} are the densities within the mixed layer and deep water portions of the profile, respectively, and h is proportional to the thickness of the transition zone between the mixed layer and deep water (Figure 3). The error function, $erf()$, dictates the density gradient in the transition zone between the mixed upper layer and stratified deeper water. Values of the four idealized parameters (ρ_{mixed}, ρ_{deep}, MLD, and h) are determined through an iterative process that minimizes the difference between $\rho(z)$ and $\rho_{obs}(z)$ in accordance with a sequential similarity detection algorithm. This metric is based upon the sum of absolute differences and was used instead of a root-mean-square deviation because of its computational efficiency and robustness [*Barnea and Silverman*, 1972].

[18] As in the work by *Steyn et al.* [1999], the multidimensional minimization was achieved with a simulated annealing algorithm [*Press et al.*, 1992]. *Kirkpatrick et al.* [1983] present a detailed explanation of the simulated annealing concept and *Press et al.* [1992] provide computer code for implementing the algorithm. In general terms, simulated annealing is a stochastic search technique for locating the global extremum of a function space. A cost function dictates whether the process seeks a minimum or maximum value. The simulated annealing algorithm is particularly good at escaping local minima and maxima.

[19] To start the simulated annealing process, an initial search space is defined that is sufficiently large. As described by *Press et al.* [1992], the search space for a function of N variables has $N + 1$ vertices. In the present case, there are four variables (ρ_{mixed}, ρ_{deep}, MLD, and h), so the search space will have five vertices, each of which represents a unique evaluation of the idealized profile (equation (5)). To create a large initial space, four of the vertices were set to extreme values that correspond to each of the variables (Figure 4a). The fifth vertex was dynamically determined for each observed profile in the WOCE data set. Specifically, ρ_{mixed} and ρ_{deep} were set to the
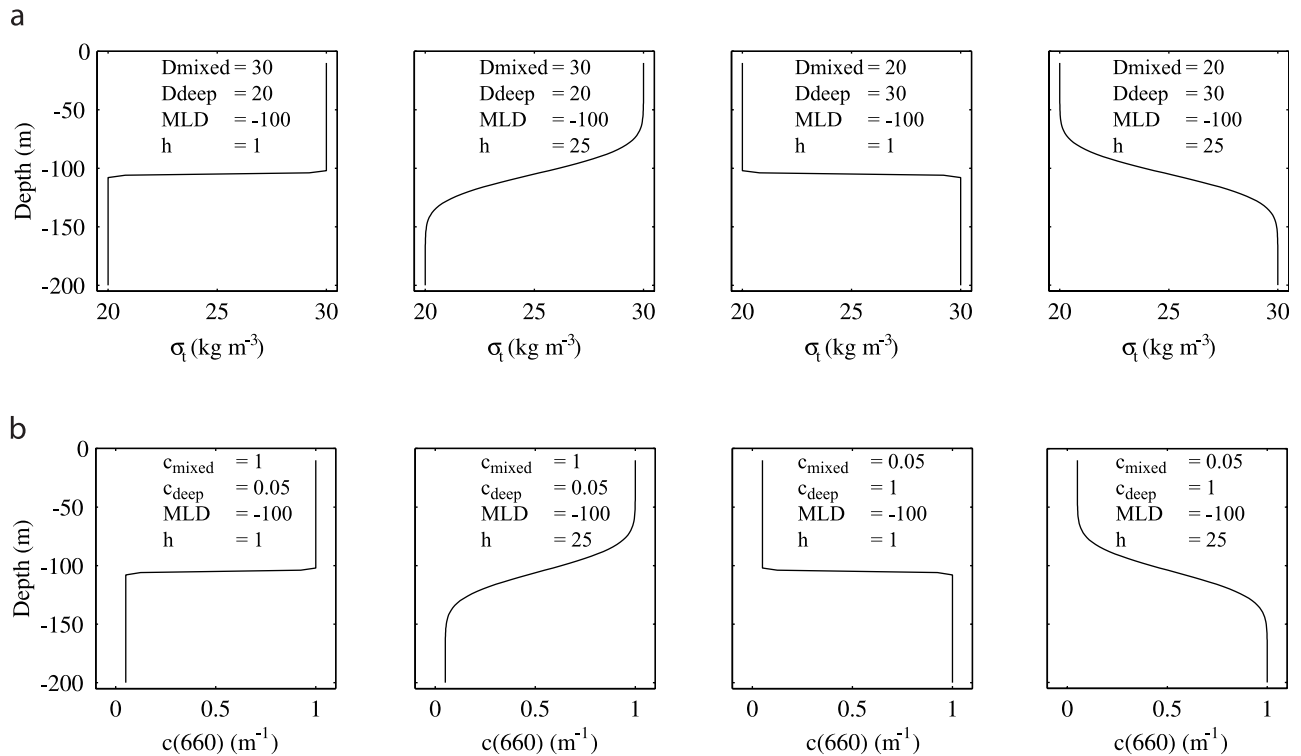
Figure 4. Initial search space for simulated annealing. Unique combinations of the four unknowns in the idealized profile equation are used to specify four of the five vertices defining the search space. Numerical values are listed in the plot of each vertex. The fifth vertex is not shown, since it was dynamically determined for each observed profile in the WOCE data set. Figures 4a and 4b depict the vertices for the Steyn and OSteyn methods, respectively.

densities at the top and bottom of the profile, respectively, MLD was set to the depth of the maximum absolute density gradient, and h was set to a depth range ±2.0% of the MLD value.

[20] The cost function used to find the parameter values is defined as

$$Cost = \sum_z |\rho_{obs}(z) - \rho(z)|, \qquad (6)$$

which represents the difference between the observed density profile, $\rho_{obs}(z)$, and the idealized profile, $\rho(z)$, on a per depth basis. Upon completion of the simulated annealing process, ρ_{mixed}, ρ_{deep}, MLD, and h will be set to values that correspond to the global minimum of equation (6), that is, to values that yield the best fit of the idealized profile to the observed one. To demonstrate the robustness of this technique, samples from each major ocean basin are plotted in Figure 5a.

[21] For convenience, the above methods are referred to as hydrographical methods, even though the Steyn algorithm was adapted from atmospheric mixed layer studies.

2.3. Algorithms for Computing MLD on the Basis of Optical Data

[22] Since no published methods for determining MLDs or scattering layer depth from profiles of beam attenuation

were found, two of the above hydrographical techniques were adapted for use with these data.

2.3.1. Method 1: Maximum Beam Attenuation Gradient (OGrad)

[23] The WOCE beam attenuation profile was smoothed with a five-point moving average and used to compute the gradient. The depth of the maximum absolute gradient magnitude, $\max |\Delta c/\Delta z|$, was considered to be the MLD. This method is the same as hydrographic method 5, but applied to optical data.

2.3.2. Method 2: Steyn Ideal Fit (OSteyn)

[24] This procedure is essentially the same as Steyn above, but with beam attenuation used instead of density. The idealized profile is a function of the four parameters c_{mixed}, c_{deep}, MLD, and h, where c_{mixed} and c_{deep} represent the beam attenuation at the top and bottom of the profile, respectively. The initial search space (Figure 4b) was created in a similar manner. A cost function in the form of equation (6) was used, but with beam attenuation substituted for density. Examples of these idealized fits are shown in Figure 5b.

[25] Both of these definitions are gradient based. The application of a fixed difference method to the $c660$ profiles is not practical because of the large range of possible values. Beam attenuation in the ocean can vary by three orders of magnitude, so it is not reasonable to apply an absolute Δc criterion. For example, *Barnard et al.* [1998] show a range of 0.02 to 1.66 m^{-1} for $c660$ for
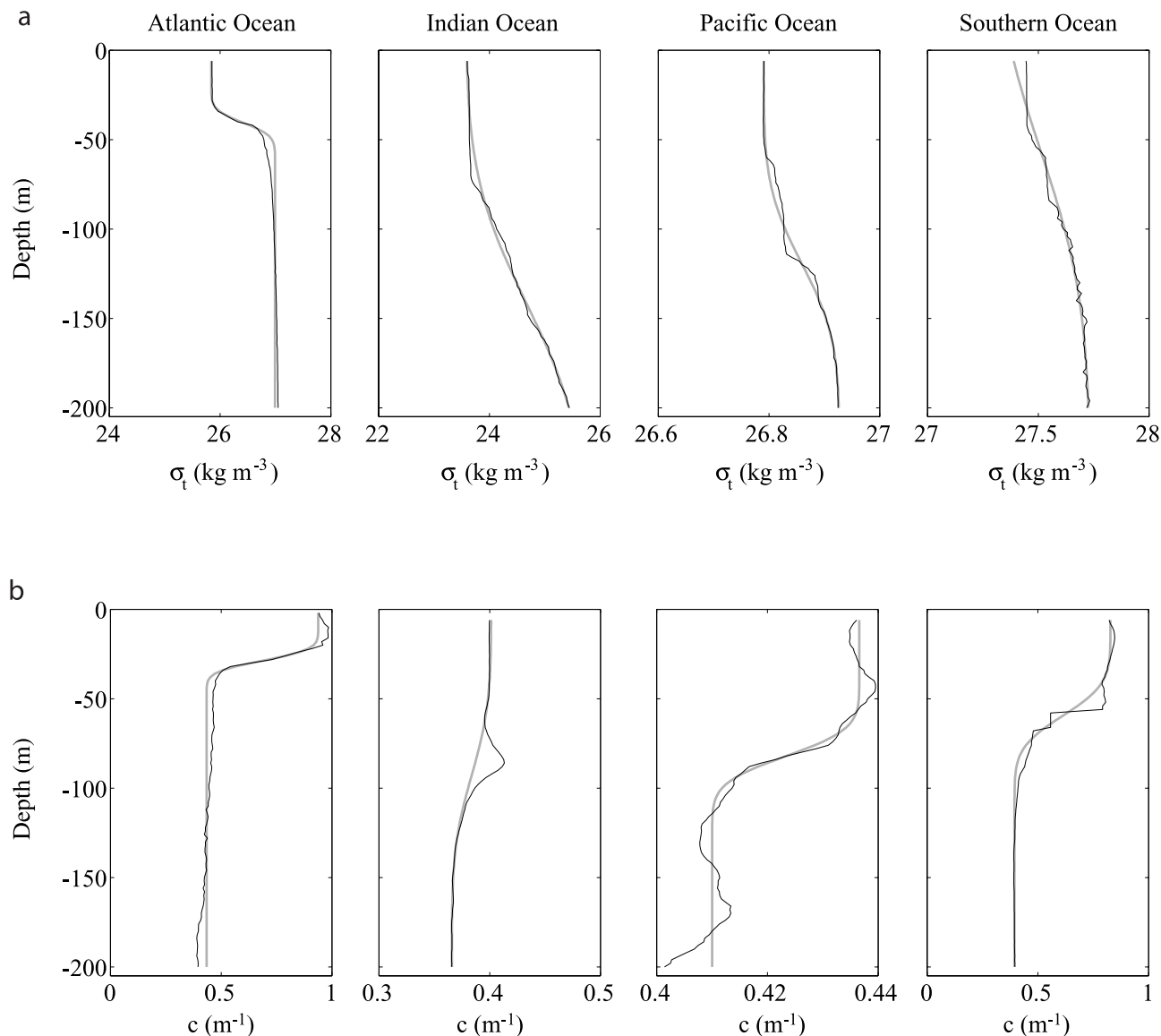
Figure 5. Comparison of idealized and observed profiles. Sample profiles corresponding to (a) density and (b) beam attenuation are depicted for each major ocean basin. Black lines are the WOCE data, and gray lines represent the optimal fit of the idealized profiles.

a global data set that excluded estuarine waters but not shelf waters.

2.4. Algorithm Comparisons

[26] The MLDs from each algorithm were compared using descriptive statistical quantities and numerical differences. The descriptive statistical measures include the mean, standard deviation, and the coefficient of variation (CV). Defined as the ratio of the standard deviation to the mean [*Zar*, 1999], the CV is a dimensionless, relative measure of dispersion, indicating the consistency of values in a series. The magnitude of the standard deviation tends to increase or decrease proportionately with similar changes in the mean. Normalizing the standard deviation by the mean removes its impact on the variability.

[27] The uncertainty between two different algorithm MLD values was expressed in two ways. The first method

used the numerical difference. The MLD uncertainty (in meters) between algorithms $A1$ and $A2$ is expressed as

$$E_1(A1, A2, i) = MLD_{A1}(i) - MLD_{A2}(i), \qquad (7)$$

where i refers to a given sample in the WOCE data set. Using this metric, intercomparisons were made between each of the six hydrographically based MLD algorithms to assess the degree of consistency amongst them. These comparisons also serve as a reference for evaluating the optically derived MLDs. In a similar fashion, differences were computed for all twelve unique pairings of hydrographic and optical algorithms, with the convention that algorithm $A1$ always referred to one of the optical methods. Second, a percent difference was defined as

Table 1. Hydrographical-Hydrographical MLD Algorithm Comparisons[a]

Algorithm Pairing	Minimum	Maximum	Median	Mean	σ	CV, %	Percent <5	Percent <10	Percent <20	Percent <50
							Hemisphere-Adjusted Summer (N = 814)			
Lev, fxGrad	0.091	79.198	5.910	7.144	8.216	114.995	27.273 (6.05)	92.383 (9.68)	96.069 (10.20)	98.894 (10.65)
Lev, Kara	0.007	54.575	2.106	4.700	7.166	152.456	74.816 (2.52)	87.224 (3.64)	94.226 (4.42)	99.754 (5.59)
fxGrad, Kara	0.002	60.628	7.294	9.117	7.951	87.204	76.904 (10.28)	93.120 (12.22)	99.017 (13.57)	
ILD, Kara	0.001	115.408	1.168	5.250	10.446	198.953	76.290 (1.65)	85.381 (2.45)	91.892 (3.39)	99.017 (5.08)
Lev, ILD	0.009	118.062	2.514	7.451	12.191	163.609	66.462 (2.48)	79.115 (3.71)	88.329 (5.20)	98.280 (7.57)
fxGrad, ILD	0.040	124.286	7.879	12.084	12.467	103.169	13.268 (6.43)	64.619 (10.61)	86.364 (13.29)	97.789 (15.94)
Grad, ILD	0.002	153.825	4.037	13.364	23.348	174.708	57.494 (3.31)	70.270 (4.47)	83.047 (6.45)	92.260 (8.34)
Grad, Kara	0.002	156.562	4.368	15.234	24.166	158.632	54.791 (3.52)	65.848 (4.74)	77.150 (6.74)	91.278 (9.79)
Grad, Steyn	0.000	183.000	4.830	14.183	20.933	147.598	50.614 (1.88)	63.145 (3.25)	75.553 (6.46)	94.963 (12.73)
Lev, Grad	0.003	160.243	5.165	18.044	26.148	144.917	49.263 (3.92)	61.057 (5.28)	73.464 (7.81)	88.206 (11.61)
fxGrad, Grad	0.000	166.000	10.000	20.477	24.604	120.155	13.145 (4.43)	39.189 (8.70)	70.639 (12.75)	89.066 (17.42)
ILD, Steyn	0.001	169.735	13.165	22.689	26.245	115.669	25.921 (2.66)	42.752 (5.16)	62.285 (9.64)	89.066 (17.62)
Kara, Steyn	0.002	174.781	16.729	25.137	26.419	105.101	21.130 (3.07)	35.872 (5.88)	55.037 (11.16)	88.206 (20.32)
Lev, Steyn	0.024	171.720	19.481	27.748	27.811	100.227	21.007 (3.20)	33.661 (5.94)	50.369 (11.82)	83.784 (22.07)
fxGrad, Steyn	1.176	181.000	21.507	30.672	26.692	87.022	3.194 (4.79)	20.025 (11.14)	45.946 (16.89)	83.170 (28.15)
							Hemisphere-Adjusted Winter (N = 297)			
Lev, fxGrad	0.012	106.128	6.162	8.788	12.522	142.490	23.232 (4.63)	88.552 (7.42)	93.266 (7.49)	97.980 (8.12)
Lev, Kara	0.417	64.368	5.705	9.504	10.576	111.270	44.108 (3.30)	70.370 (4.37)	87.542 (5.95)	98.990 (8.21)
fxGrad, Kara	0.115	81.664	8.952	12.225	11.708	95.770	13.468 (1.58)	60.943 (8.39)	86.869 (10.21)	97.306 (12.43)
Grad, Steyn	0.000	102.454	6.002	12.764	19.071	149.410	47.811 (0.91)	64.646 (1.80)	79.461 (3.39)	94.613 (6.35)
ILD, Kara	0.017	63.518	3.767	10.744	14.278	132.890	54.882 (1.05)	67.677 (1.80)	78.788 (3.71)	96.633 (8.25)
Grad, ILD	0.032	117.768	7.608	14.536	17.999	123.830	40.741 (1.73)	58.249 (2.83)	77.104 (4.45)	92.593 (7.38)
Lev, ILD	0.026	65.958	8.414	16.794	17.818	106.100	38.047 (1.74)	53.872 (2.88)	67.003 (5.40)	93.266 (12.88)
fxGrad, ILD	0.038	73.477	11.123	19.611	18.347	93.560	12.458 (1.37)	46.128 (5.33)	65.993 (7.63)	88.889 (14.51)
ILD, Steyn	0.011	126.839	14.487	21.426	21.638	100.990	23.232 (1.44)	38.384 (2.61)	62.290 (5.69)	88.889 (10.81)
Grad, Kara	0.069	114.448	13.123	22.047	22.457	101.860	31.650 (2.07)	43.771 (2.89)	57.239 (4.36)	86.195 (11.55)
fxGrad, Grad	2.000	93.000	18.000	28.347	24.221	85.440	8.081 (1.42)	23.569 (4.00)	52.189 (7.02)	78.451 (14.23)
Lev, Grad	0.009	138.128	18.612	27.821	26.274	94.440	26.936 (1.93)	40.067 (3.12)	50.842 (4.84)	79.125 (13.55)
Kara, Steyn	0.436	127.525	23.772	27.894	22.383	80.240	13.131 (1.50)	24.916 (3.32)	42.761 (6.17)	86.532 (16.74)
fxGrad, Steyn	0.245	124.999	31.341	33.778	24.937	73.830	7.407 (2.12)	22.222 (3.22)	36.027 (5.28)	76.431 (19.61)
Lev, Steyn	0.009	149.764	30.152	33.102	25.646	77.480	16.835 (1.22)	22.222 (2.36)	34.007 (5.17)	77.778 (18.82)

[a]The numerical differences between MLDs associated with pairs of algorithms were computed and grouped according to hemispherically corrected season (summer and winter). Only MLDs that were less than the corresponding profile depth were used in the difference calculations. Data in columns labeled Percent <5, 10, 20, and 50 refer to the percentage of MLD values that differed by less than 5, 10, 20, and 50 m, respectively. The value in parentheses is the average percent difference, which indicates the degree of dissimilarity between the MLDs from two algorithms. Smaller percentages are better. Algorithm pairings are sorted according to the <20 m difference criterion.

$$E_2(A1, A2, i) = \frac{|MLD_{A1}(i) - \text{mean}(A1, A2, i)|}{\text{mean}(A1, A2, i)} \times 100\%,$$

where

$$\text{mean}(A1, A2, i) = \frac{MLD_{A1}(i) + MLD_{A2}(i)}{2}.$$

(8)

Because there is no correct value, the mean between two MLDs being compared was used as the "correct" MLD value. Percent differences were computed for all unique pairings of hydrographic-hydrographic and hydrographic-optical algorithms.

[28] A final set of algorithm comparisons was made on the basis of linear least squares analysis of subsets of MLD values. The subdivisions correspond to five difference criteria (<5 m, <10 m, <20 m, <50 m, and <200 m) for each of two seasonal designations (summer and winter). The best and worst hydrographical-hydrographical and hydro-graphical-optical algorithm pairings were determined by ranking the product of the least squares coefficient of determination (r^2) and the percentage of MLD values satisfying a given difference criterion. The r^2 values were weighted in this manner to strike a balance between instances with a high r^2 involving a small number of MLDs and those with a low r^2 encompassing a larger percentage of MLD values.

2.5. Filtering of MLD Values

[29] Among the sampling stations, profile depths ranged from 84–200 m, with 1,798 (86%) extending to 200 m. For each of these stations, 8 mixed layer depths were computed using the 6 hydrographically based methods and 2 optically based methods. To avoid biasing the distribution of MLD values, if any of the 8 values was equal to the profile depth, all data associated with that sampling station were omitted from the analysis. This filtering step reduced the number of sampling stations from 2,085 to 1,803.

[30] For seasonal analysis, summer was defined as June–August in the northern hemisphere and December–February in the southern hemisphere. Winter was defined as December–February in the northern hemisphere and June–August in the southern hemisphere. As a result of these assignments, 814 of the 1,803 (45%) available stations were sampled in summer and 297 (16%) were sampled in winter.

3. Results

[31] After filtering according to season, the mean, median, and standard deviation were computed for the MLDs derived from each of the six hydrographic algorithms (Table 1) and both optical algorithms (Table 2). When plotted, these descriptive statistics reveal several patterns

Table 2. Optical-Hydrographical MLD Algorithm Comparisons[a]

Algorithm Pairing	Minimum	Maximum	Median	Mean	σ	CV, %	Percent <5	Percent <10	Percent <20	Percent <50
					Hemisphere-Adjusted Summer (N = 814)					
OGrad, ILD	0.064	174.332	10.964	19.958	23.372	117.110	31.327 (2.97)	47.052 (5.37)	66.093 (9.02)	89.066 (14.87)
OGrad, Grad	0.000	172.000	10.000	22.608	28.583	126.430	34.889 (2.65)	46.806 (4.19)	64.005 (7.60)	82.924 (12.77)
OGrad, Kara	0.007	174.545	12.701	21.089	23.615	111.980	30.221 (3.06)	45.086 (5.63)	62.285 (9.47)	88.206 (15.92)
OGrad, Lev	0.021	175.070	12.337	22.457	25.258	112.470	30.221 (3.00)	44.840 (5.79)	61.671 (9.53)	85.749 (16.64)
OSteyn, ILD	0.009	175.320	14.979	22.912	23.537	102.730	22.973 (2.74)	36.855 (4.61)	60.565 (9.54)	88.084 (16.92)
OSteyn, Grad	0.008	172.989	13.774	24.755	27.421	110.770	23.587 (2.28)	39.189 (4.36)	59.828 (8.48)	84.029 (15.38)
OSteyn, Steyn	0.003	174.947	17.415	26.821	27.680	103.200	20.762 (2.42)	34.398 (4.37)	54.177 (7.48)	83.170 (14.94)
OGrad, fxGrad	0.000	182.000	16.000	26.431	26.717	101.080	15.111 (4.51)	32.924 (8.20)	53.931 (13.20)	83.538 (21.78)
OSteyn, Kara	0.067	175.534	18.008	25.136	23.486	93.430	18.305 (2.80)	30.958 (5.51)	53.317 (11.05)	87.101 (19.39)
OGrad, Steyn	0.005	179.000	17.254	27.368	29.341	107.210	23.464 (2.60)	38.084 (4.51)	53.194 (8.19)	82.432 (16.73)
OSteyn, Lev	0.015	176.059	18.492	26.672	24.891	93.320	17.076 (2.63)	30.835 (5.80)	53.071 (11.47)	84.275 (20.50)
OSteyn, fxGrad	0.038	182.989	22.836	31.257	26.010	83.210	7.248 (3.56)	19.533 (7.36)	43.366 (14.83)	80.713 (25.97)
					Hemisphere-Adjusted Winter (N = 297)					
OSteyn, ILD	0.042	101.608	11.367	16.569	16.367	98.780	24.916 (1.57)	45.118 (2.93)	70.034 (5.54)	95.623 (10.17)
OSteyn, Grad	0.023	129.474	11.233	19.192	22.841	119.010	25.253 (1.48)	45.455 (2.94)	70.034 (5.31)	91.246 (8.38)
OGrad, ILD	0.006	101.477	11.646	16.762	16.934	101.030	26.599 (1.72)	45.118 (2.86)	68.013 (5.16)	95.286 (10.39)
OGrad, Grad	0.000	134.000	12.000	20.209	24.179	119.650	26.599 (1.51)	41.414 (2.55)	64.983 (4.93)	90.236 (8.83)
OGrad, Steyn	0.040	150.999	15.183	24.735	25.749	104.100	18.855 (1.69)	35.017 (2.97)	59.596 (5.55)	86.195 (10.33)
OSteyn, Steyn	0.045	144.585	15.096	23.413	24.404	104.230	19.865 (1.54)	35.690 (2.85)	59.259 (5.31)	87.542 (9.92)
OSteyn, Kara	0.254	103.298	18.124	22.998	19.159	83.310	18.519 (1.88)	31.313 (3.08)	55.219 (6.18)	89.899 (14.46)
OGrad, Kara	0.062	103.025	18.336	23.033	19.155	83.160	17.508 (1.73)	29.630 (2.84)	54.545 (6.62)	89.562 (14.66)
OGrad, Lev	0.057	105.155	19.901	25.181	21.140	83.950	17.172 (1.40)	30.640 (3.49)	50.168 (6.71)	84.512 (15.61)
OSteyn, Lev	0.123	105.428	20.475	25.705	21.092	82.050	16.162 (1.64)	29.966 (2.99)	49.158 (6.03)	84.848 (15.93)
OSteyn, fxGrad	0.041	123.722	22.134	29.318	23.693	80.810	15.488 (1.63)	25.253 (2.90)	46.128 (6.30)	77.104 (15.91)
OGrad, fxGrad	0.000	130.000	22.000	28.758	23.960	83.320	17.508 (2.17)	26.263 (3.10)	43.771 (6.35)	77.441 (15.74)

[a]The numerical differences between MLDs associated with pairs of algorithms were computed and grouped according to hemispherically corrected season (summer and winter). Only MLDs that were less than the corresponding profile depth were used in the difference calculations. Data in columns labeled Percent <5, 10, 20, and 50 refer to the percentage of MLD values that differed by less than 5, 10, 20, and 50 m, respectively. The value in parentheses is the average percent difference, which indicates the degree of dissimilarity between the MLDs from two algorithms. Smaller percentages are better. Algorithm pairings are sorted according to the <20 m difference criterion.

(Figure 6). Because of stronger mixing, MLDs are consistently deeper in winter than summer. In general, fxGrad and Lev produced the shallowest MLDs, irrespective of season, while Grad, Steyn and the two optical methods tended to yield deeper MLDs. ILD and Kara values lie in between these bounds. These groupings reflect the similarities and differences among the different algorithmic definitions of the mixed layer depth. For example, the behavior of the Steyn algorithms is attributable to the chosen parameterization of the idealized profile. Defining the MLD to be at the top of the transition zone (Figure 3) would probably improve the correlation between Steyn/OSteyn and the other methods. Also noteworthy is the fact that the Steyn algorithms focus on fitting the overall shape of a profile, at the expense of finer-scale features (Figures 5a and 5b).

[32] Another way to view the differences between algorithms is to consider the percentage of MLD points that satisfy a given difference criterion. Taking the seasonal analysis further, hydrographic-hydrographic and hydrographic-optical algorithm comparisons were made on the basis of difference criteria of <5 m, <10 m, <20 m, and <50 m (Tables 1 and 2). In general, the top five pairings are reasonably consistent for all difference criteria, regardless of season. The interhydrographic results reveal slightly stronger agreement in summer, while the converse is true for the hydrographic-optical algorithms.

[33] Among the hydrographic-hydrographic pairings, Lev-fxGrad and Lev-Kara exhibit the smallest differences in both summer and winter. Of the two, Lev-Kara has the smallest percent difference (typically <6%) for all tested criteria, except for differences <50 m in winter. Combina-

tions involving optical algorithms, however, show seasonal dependencies. OGrad paired with either Grad or ILD produced the best results in summer, while OSteyn teamed with either Grad or ILD yielded the smallest differences in winter. Note that the top performing hydrographic algorithms are the same in both instances. Results for Grad coupled with OGrad (summer) or OSteyn (winter) generally have the smallest percent differences, ranging from 1.48% to 12.77%, depending on the difference criterion. The coefficients of variation are disappointingly large in all instances (>100%). This statistic is a relative measure of dispersion that reflects the inconsistency of values in a series. The effect of these CVs is evident in the variability among MLD algorithms as plotted in Figure 6.

[34] Considering the top five interhydrographical pairings (Table 1), MLDs agree to within 50 m nearly 100% of the time, irrespective of season. Better than 90% of MLDs in summer and 80% in winter satisfy the <20 m difference criterion. As for the top five hydrographical-optical pairings (Table 2), nearly 90% of the MLDs lie within 50 m and better than 60% are within 20 m of one another, regardless of season. The hydrographical-optical results are particularly encouraging given that both optical MLD definitions (1) are based on a gradient criterion for beam attenuation profiles and (2) tend to produce larger depths.

[35] A final series of comparisons was made by performing a linear least squares fit on subsets of MLD values corresponding to the same difference criteria and seasonal designations. For the hydrographical-hydrographical pairings (Table 3), the best summer results have r^2 values ≥ 0.9 and usually involve the Lev-fxGrad algorithm. The worst
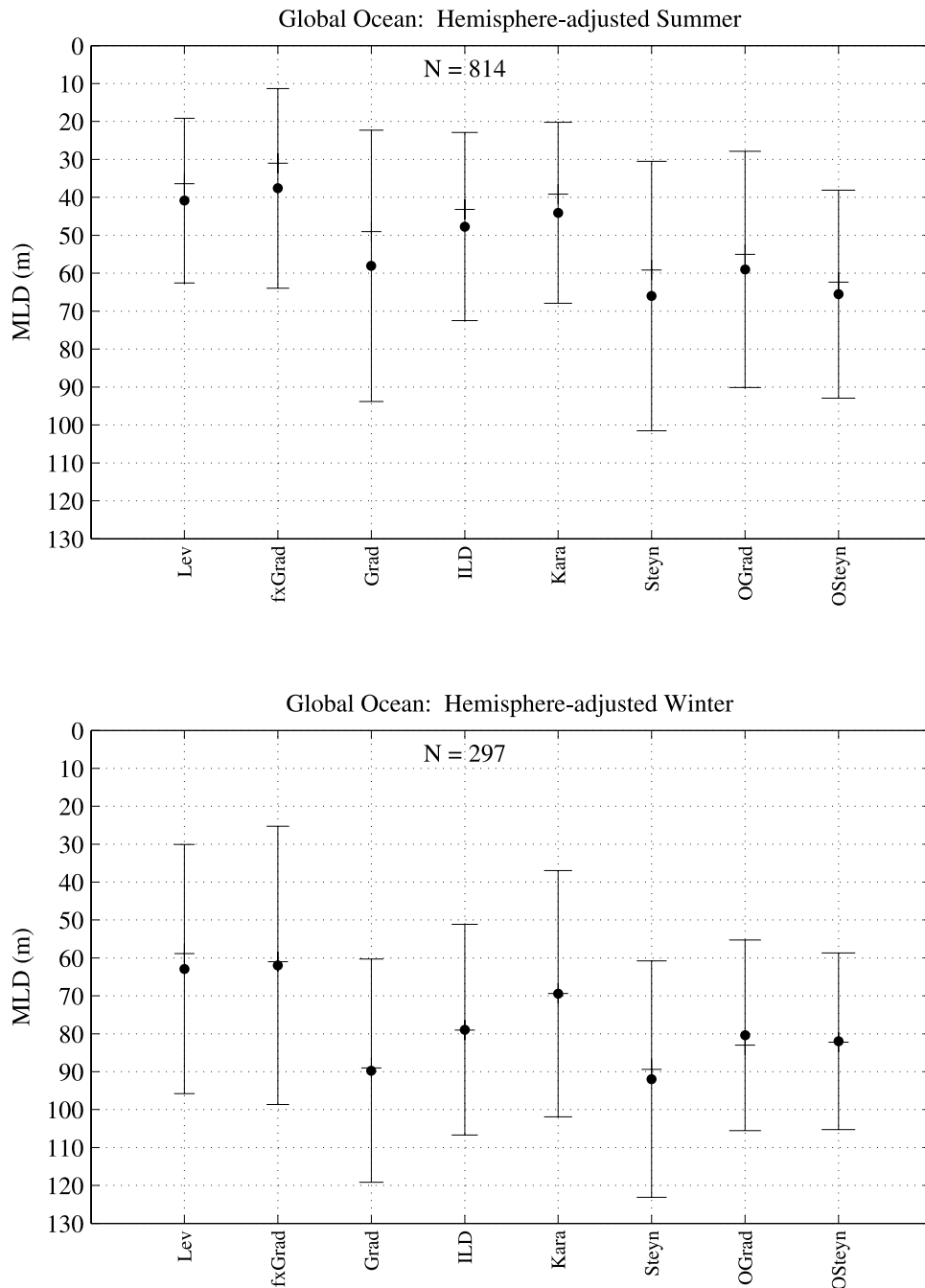
Figure 6. Seasonally adjusted, global ocean, mixed layer depths. MLDs are grouped according to hemispherically adjusted summer and winter periods. The mean (dots), median (short horizontal lines), and standard deviation (line length = ±1σ) of the MLDs computed with each algorithm are plotted for both seasons.

pairings consist of Steyn coupled with either fxGrad or Kara. In winter, Lev-fxGrad is typically the best pairing and r^2 values are also ≥ 0.9. The worst winter pairings consist of Steyn and either fxGrad or Kara.

[36] Regarding the hydrographical-optical algorithm pairings (Table 4), optimal combinations for summer data are either Grad-OGrad or ILD-OGrad, having r^2 values >0.9 for difference criteria as large as 20 m. The corresponding worst pairing is always fxGrad-OSteyn. In winter, the best results are associated with either ILD-OGrad or ILD-

OSteyn. For difference criteria as large as 20 m, r^2 values range from 0.87 to 0.98. Again, fxGrad-OSteyn tends to be the worst pairing.

[37] The degree of correlation between the pairings is more easily interpreted graphically. For example, consider the best and worst hydrographical-hydrographical pairs (Table 3) and the best hydrographical-optical pair (Table 4) satisfying the <20 m difference criterion for both summer and winter. All MLD values derived from these algorithms are plotted (Figures 7 and 8) to illustrate the spread in the

Table 3. Best and Worst Combinations Among the Hydrographical MLD Algorithms for Various Difference Criteria Using World Ocean Data

Difference Criterion, m	Best Algorithm Pairing (r^2), % of MLDs	Worst Algorithm Pairing (r^2), % of MLDs
	Summer	
<5	ILD-Kara (0.994, 76.29)	fxGrad-Steyn (0.998, 3.19)
<10	Lev-fxGrad (0.982, 92.38)	fxGrad-Steyn (0.988, 20.03)
<20	Lev-fxGrad (0.963, 96.07)	fxGrad-Steyn (0.963, 45.95)
<50	Lev-fxGrad (0.901, 98.89)	Kara-Steyn (0.576, 88.21)
<200	Lev-fxGrad (0.890, 100)	Kara-Steyn (0.285, 100)
	Winter	
<5	ILD-Kara (0.989, 54.88)	fxGrad-Steyn (0.983, 7.41)
<10	Lev-fxGrad (0.993, 88.55)	fxGrad-Steyn (0.988, 22.22)
<20	Lev-fxGrad (0.980, 93.27)	Lev-Steyn (0.926, 34.01)
<50	Lev-fxGrad (0.929, 97.98)	Kara-Steyn (0.637, 86.53)
<200	Lev-fxGrad (0.856, 100)	Kara-Steyn (0.309, 100)

data. Dashed lines delineate the 20 m accuracy limit asserted by *Kara et al.* [2000]. Points between these lines represent MLDs that differ by less than 20 m. Data lying outside of the dashed lines were excluded from the least squares analysis. Although not as strongly correlated, the best hydrographical-optical pairings fall within the extremes of the interhydrographic combinations. This pattern is also evident in Tables 1–4.

4. Discussion

[38] The goal of this study was to investigate the potential for determining oceanic mixed layer depths from profiles of total beam attenuation at 660 nm, *c*660. Two different gradient-based algorithms were developed to derive MLDs from the *c*660 profiles. To evaluate the merit of these approaches, the optically derived MLDs were compared to MLDs computed with more "conventional" algorithms utilizing temperature or density profiles.

[39] For all scenarios pertaining to the hydrographical intercomparisons, the best pairings involved two fixed difference algorithms (Table 3), indicating the consistency of MLDs derived from them. In fact, the Lev-fxGrad combination is the strongest pairing. This result does not imply that these two algorithms are more accurate or superior to the others, but rather that Lev and fxGrad are more strongly correlated than all other unique hydrographical-hydrographical combinations. All of the worst pairings consisted of Steyn with either fxGrad or Kara, which is attributable to their different approaches in computing the mixed layer depth, that is, ideal fit versus fixed difference. The hydrographical-optical results were similarly dominated by a few pairings (Table 4). Grad-OGrad produced the best results for the majority of cases, which is not surprising given that both represent gradient-based algorithms. What was unexpected, however, is how favorably ILD compared to OGrad and OSteyn, since these pairs represent fixed difference to gradient-based algorithm combinations. Notwithstanding these two pairings, combinations between algorithms based on fundamentally different strategies generally yielded the poorest results. Of these types of pairings, fxGrad-OSteyn faired the worst in the majority of cases.

[40] The quality of the algorithm pairings is more apparent when the data are presented graphically. Plots

corresponding to the best hydrographical-hydrographical pairs in both summer and winter (Figures 7 and 8, respectively) show that the MLDs are more tightly clustered than those for the best hydrographical-optical pair. This pattern is indicative of the higher r^2 values associated with the hydrographical-hydrographical pairings (Tables 3 and 4). Plots of the worst hydrographical-hydrographical pairs clearly show how large the disparity can be between the various algorithms. Also evident is the tendency of the Steyn algorithm to produce deeper MLDs, a propensity also present in the global, seasonal MLD plots (Figure 6). Finally, there does not appear to be any ocean basin clustering. For a given season, MLDs from each ocean basin generally span a similar range.

[41] Several factors account for much of the disparity between the hydrographical and optical MLD algorithms. First, the inherent fluctuations of the mixed layer depth limit the accuracy of its determination to 20 m for 85% of possible instances, regardless of the algorithm used [*Kara et al.*, 2000]. The results of this study support this level of accuracy. We obtained median differences of approximately 6 m and 11 m for the best interhydrographical and hydrographical-optical pairs, respectively, for both seasons. Also adding to the variability are different mathematical formulations, most notably, fixed difference methods versus gradient methods. A third issue is the susceptibility of optical parameters to biological influences. The optical algorithms are based on profiles of beam attenuation at 660 nm which, in the open ocean, are largely attributable to the concentration of suspended particles, both alive and inanimate [*Pak et al.*, 1988]. The effects of biological processes (e.g., primary production, grazing, sinking, swimming, aggregation, and photoadaptation) can impact *c*660 profiles in ways that are only indirectly related to physical forcing. Growth and predation can occur even when the hydrographical parameters are constant in time. A final contributing factor to the discrepancies pertains to the parameters used to estimate the mixed layer depth. In the hydrographic case, the physical parameters directly influence the dynamics associated with the MLD (e.g., lateral restratification). The optical parameters, on the other hand, are largely passive, being advected with the flow [*Chang and Dickey*, 2004].

Table 4. Best and Worst Combinations Between All Possible Unique Combinations of Hydrographical and Optical MLD Algorithms for Various Difference Criteria Using World Ocean Data

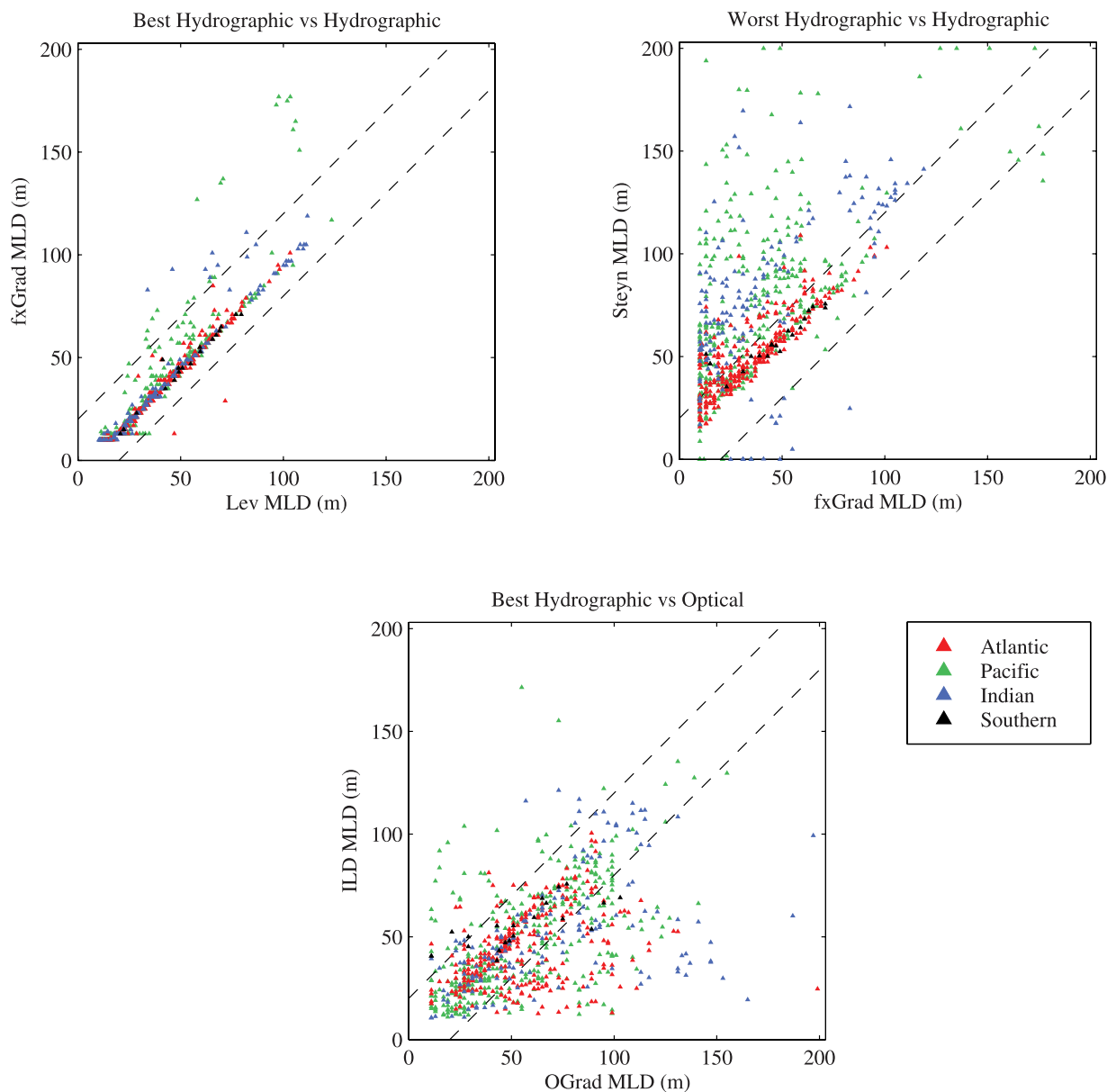| Difference Criterion, m	Best Algorithm Pairing (r^2), % of MLDs	Worst Algorithm Pairing (r^2), % of MLDs
	Summer	
<5	Grad-OGrad (0.988, 34.89)	fxGrad-OSteyn (0.984, 7.25)
<10	Grad-OGrad (0.963, 46.81)	fxGrad-OSteyn (0.950, 19.53)
<20	ILD-OGrad (0.880, 66.09)	fxGrad-OSteyn (0.881, 43.37)
<50	Lev-OGrad (0.666, 85.75)	Steyn-OSteyn (0.415, 83.17)
<200	Lev-OGrad (0.261, 100)	Steyn-OSteyn (0.073, 100)
	Winter	
<5	Grad-OGrad (0.977, 26.60)	fxGrad-OSteyn (0.987, 15.49)
<10	ILD-OSteyn (0.953, 45.12)	fxGrad-OSteyn (0.961, 25.25)
<20	Grad-OSteyn (0.868, 70.03)	fxGrad-OGrad (0.843, 43.77)
<50	ILD-OGrad (0.636, 95.29)	Steyn-OSteyn (0.436, 87.54)
<200	Lev-OGrad (0.364, 100)	Steyn-OSteyn (0.087, 100)

Figure 7. Best and worst algorithm pairings during summer (hemispherically corrected). On the basis of the least squares analysis (Tables 3 and 4), MLDs corresponding to the best/worst interhydrographical algorithm pair are plotted against one another for the summer season. For comparison purposes, MLDs for the best hydrographical-optical pair are shown in the bottom plot. Points located within the dashed lines correspond to MLD pairs that differ by <20 m.

[42] In spite of these differences, the optical algorithms are in first-order agreement with the conventional hydrographical methods. Higher correlation between the hydrographical and optical techniques may be possible at certain times of day, such as early morning hours, when the upper water column is well mixed and phytoplankton photosynthesis is not operating at peak levels. *Siegel et al.* [1989], *Gardner et al.* [1993, 1995], and *Walsh et al.* [1995], among others, have shown that the diel signal can be strong. In this study, the use of archived data precluded the optimization of sampling times. Future experiments should pay close attention to the periods during which growth and predation are minimal, so that the bio-optical and physical structures are driven by the same forcing factors.

[43] Of the two optical techniques, OGrad was more strongly correlated with the conventional methods, in particular Grad (Tables 2 and 4). This result suggests that, to a large extent, the vertical distribution of particles is governed by density structure or by parameters that are indirectly associated with it, such as nutrients. Optimizing the algorithms for regional conditions by means of simultaneously obtained hydrographic and attenuation profiles collected at specific times of the diel cycle would potentially increase
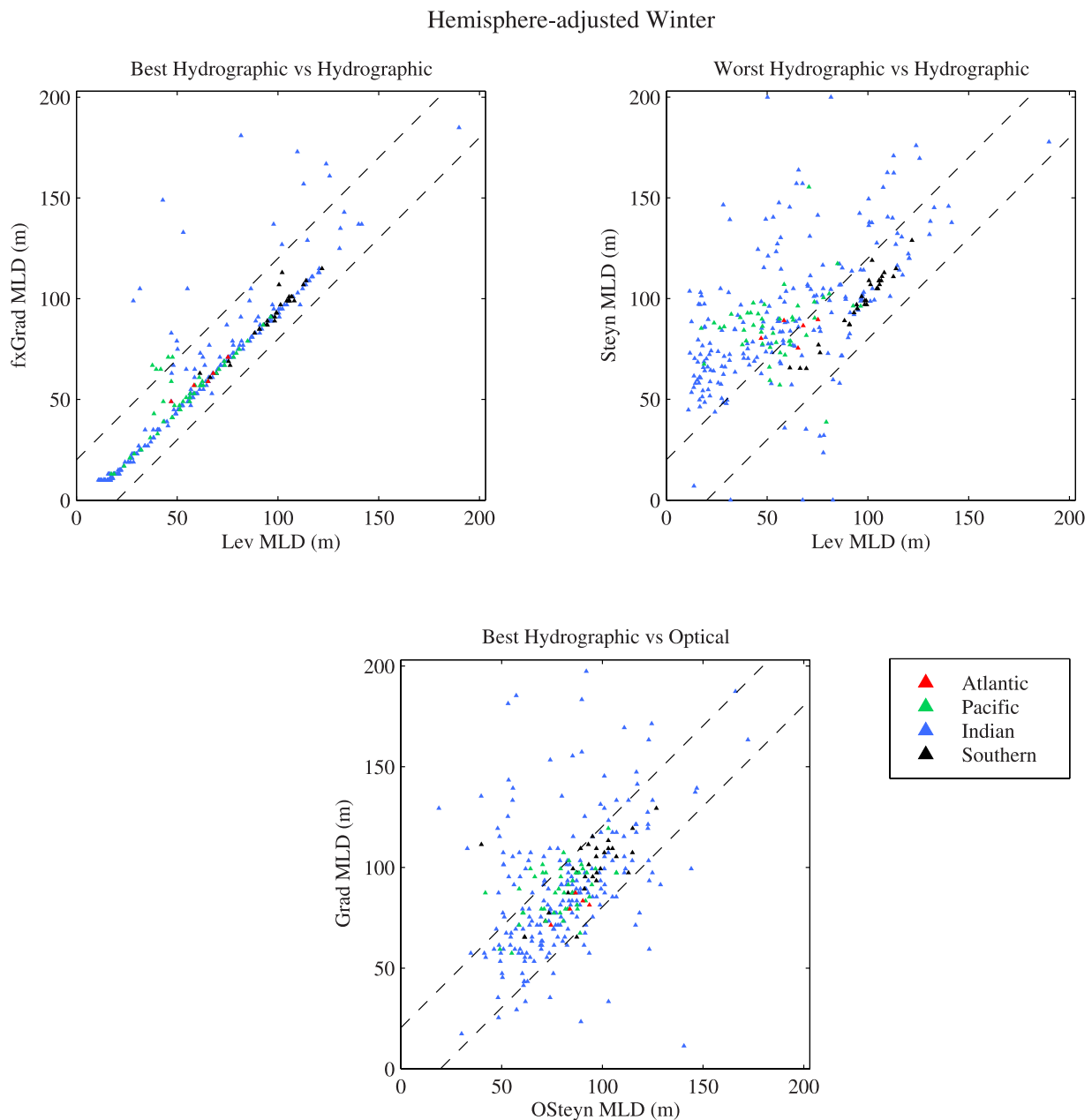
Figure 8. Best and worst algorithm pairings during winter (hemispherically corrected). On the basis of the least squares analysis (Tables 3 and 4), MLDs corresponding to the best/worst interhydrographical algorithm pair are plotted against one another for the winter season. For comparison purposes, MLDs for the best hydrographical-optical pair are shown in the bottom plot. Points located within the dashed lines correspond to MLD pairs that differ by <20 m.

the correlation between hydrographically and optically derived MLDs.

References

Ali, M. M., and R. Sharma (1994), Estimation of mixed layer depth in the equatorial Indian Ocean using GEOSAT altimeter data, *Mar. Geod.*, *17*(1), 63–72.

Barnard, A. H., W. S. Pegau, and J. R. V. Zaneveld (1998), Global relation-ships of the inherent optical properties of the oceans, *J. Geophys. Res.*, *103*(C11), 24,955–24,968.

Barnea, D. I., and H. F. Silverman (1972), A class of algorithms for fast digital image registration, *IEEE Trans. Comput.*, *C-21*(2), 179–186.

Behrenfeld, M. J., and P. G. Falkowski (1997), Photosynthetic rates derived from satellite-based chlorophyll concentration, *Limnol. Oceanogr.*, *42*(1), 1–20.

Brainerd, K. E., and M. C. Gregg (1995), Surface mixed and mixing layer depths, *Deep Sea Res., Part I*, *42*, 1521–1543.

Chang, G. C., and T. D. Dickey (2004), Coastal ocean optical influences on solar transmission and radiant heating rate, *J. Geophys. Res.*, *109*, C01020, doi:10.1029/2003JC001821.

Durand, F., L. Gourdeau, T. Delcroix, and J. Verron (2003), Can we im-prove the representation of modeled ocean mixed layer by assimilating surface-only satellite-derived data? A case study for the tropical Pacific

during the 1997–1998 El Niño, *J. Geophys. Res.*, *108*(C6), 3200, doi:10.1029/2002JC001603.

Gardner, W. D., I. D. Walsh, and M. J. Richardson (1993), Biophysical forcing of particle production and distribution during a spring bloom in the North Atlantic, *Deep Sea Res., Part II*, *40*, 171–195.

Gardner, W. D., S. P. Chung, M. J. Richardson, and I. D. Walsh (1995), The oceanic mixed-layer pump, *Deep Sea Res., Part II*, *42*, 757–775.

Gardner, W. D., J. S. Gundersen, M. J. Richardson, and I. D. Walsh (1999), The role of seasonal and diel changes in mixed-layer depth on carbon and chlorophyll distributions in the Arabian Sea, *Deep Sea Res., Part II*, *46*, 1833–1858.

Hoge, F. E., C. W. Wright, W. B. Krabill, R. R. Buntzen, G. D. Gilbert, R. N. Swift, J. K. Yungel, and R. E. Berry (1988), Airborne lidar detection of subsurface oceanic scattering layers, *Appl. Opt.*, *27*(19), 3969–3977.

Kara, A. B., P. A. Rochford, and H. E. Hurlburt (2000), Mixed layer depth variability and barrier layer formation over the North Pacific Ocean, *J. Geophys. Res.*, *105*(C7), 16,783–16,801.

Kirkpatrick, S., C. D. Gelatt, and M. P. Vecchi (1983), Optimization by simulated annealing, *Science*, *220*(4598), 671–680.

Kraus, E. B., and J. A. Businger (1994), *Atmosphere-Ocean Interaction*, Oxford Univ. Press, New York.

Lee, C. M., B. H. Jones, K. H. Brink, and A. S. Fischer (2000), The upper-ocean response to monsoonal forcing in the Arabian Sea: Seasonal and spatial variability, *Deep Sea Res., Part II*, *47*, 1177–1226.

Lee, K. J., Y. Park, A. Bunkin, R. Nunes, S. Pershin, and K. Voliak (2002), Helicopter-based lidar system for monitoring the upper ocean and terrain surface, *Appl. Opt.*, *41*(3), 401–406.

Levitus, S. (1982), Climatological atlas of the world ocean, *NOAA Prof. Pap. 13*, 173 pp.

Lukas, R., and E. Lindstrom (1991), The mixed layer of the western equatorial Pacific Ocean, *J. Geophys. Res.*, *96*(Supplement), 3343–3357.

Millero, F. J., and A. Poisson (1981), International one-atmosphere equation of state of seawater, *Deep Sea Res., Part A*, *28*, 625–629.

Pak, H., D. A. Kiefer, and J. C. Kitchen (1988), Meridional variations in the concentration of chlorophyll and microparticles in the North Pacific Ocean, *Deep Sea Res., Part A*, *35*, 1151–1171.

Press, W. H., S. A. Teukolsky, W. T. Vetterling, and B. P. Flannery (1992), *Numerical Recipes in C*, Cambridge Univ. Press, New York.

Price, J. F., R. A. Weller, and R. Pinkel (1986), Diurnal cycling: Observations of the upper ocean response to diurnal heating, cooling, and wind mixing, *J. Geophys. Res.*, *91*(C7), 8411–8427.

Siegel, D. A., T. D. Dickey, L. Washburn, M. K. Hamilton, and B. G. Mitchell (1989), Optical determination of particulate abundance and production variations in the oligotrophic ocean, *Deep Sea Res., Part A*, *36*, 211–222.

Steyn, D. G., M. Baldi, and R. M. Hoff (1999), The detection of mixed layer depth and entrainment zone thickness from lidar backscatter profiles, *J. Atmos Oceanic Technol.*, *16*, 953–959.

Walsh, I. D., S. P. Chung, M. J. Richardson, and W. D. Gardner (1995), The diel cycle in the integrated particle load in the equatorial Pacific: A comparison with primary production, *Deep Sea Res., Part II*, *42*, 465–478.

Yan, X.-H., J. R. Schubel, and D. W. Pritchard (1990), Oceanic upper mixed layer depth determination by the use of satellite data, *Remote Sens. Environ.*, *32*(1), 55–74.

Zar, J. H. (1999), *Biostatistical Analysis*, Prentice-Hall, Upper Saddle River, N. J.

————————————————

E. Boss, School of Marine Sciences, University of Maine, Libby Hall, Orono, ME 04469, USA.

W. D. Gardner, A. V. Mishonov, and M. J. Richardson, Department of Oceanography, Texas A&M University, College Station, TX 77843, USA.

J. R. V. Zaneveld, WET Labs, Inc., 620 Applegate St., Philomath, OR 97370, USA.

D. G. Zawada, Center for Coastal and Watershed Studies, U.S. Geological Survey, 600 Fourth Street South, St. Petersburg, FL 33701, USA. (dzawada@usgs.gov)